

## Article

# Recognition of *Aedes aegypti* Mosquito Saliva Protein LTRIN by the Human Receptor $LT\beta R$ for Controlling the Immune Response

Su Ning Loh<sup>1</sup>, Ian Russell Anthony<sup>1</sup>, Edem Gavor<sup>1</sup>, Xin Shan Lim<sup>1</sup>, R. Manjunatha Kini<sup>1,2</sup>, Yu Keung Mok<sup>1,\*</sup> and J. Sivaraman<sup>1,\*</sup>

<sup>1</sup> Department of Biological Sciences, National University of Singapore, 14 Science Drive 4, Singapore 117543, Singapore; e0383794@u.nus.edu (S.N.L.)

<sup>2</sup> Department of Pharmacology, Yong Loo Lin School of Medicine, National University of Singapore, Singapore 117600, Singapore

\* Correspondence: dbsmikh@nus.edu.sg (Y.K.M.); dbsjaya@nus.edu.sg (J.S.)

**Simple Summary:** In this study, we present the characterization of *Aedes aegypti* mosquito salivary protein, LTRIN (lymphotoxin  $\beta$  receptor inhibitor), a key facilitator of ZIKV transmission. Injected into the human host during blood-feeding, LTRIN interacts with the human receptor  $LT\beta R$ . We found that LTRIN exists as a thermostable protein with homodimers consisting of an alpha helix-dominant secondary structure with two EF-hand motifs, crucial for withstanding temperature fluctuations during blood-feeding. Despite being an EF-hand protein, its secondary structure remains unaffected by  $Ca^{2+}$  binding. ELISA assays and HDX-MS experiments identified the binding region of LTRIN with  $LT\beta R$ . Disrupting the calcium-binding ability in the second EF-hand motif significantly impacted the interaction between LTRIN, particularly the 15 kDa C-terminal protein,  $\Delta LTRIN$ , and  $LT\beta R$ . Moreover, the decrease in binding affinity of full-length LTRIN suggests the presence of only the truncated form,  $\Delta LTRIN$ , in the mosquito's saliva, as the N-terminal region likely covers the interaction site. This insight provides a basis for developing inhibitors against LTRIN as a potential treatment or vaccine target for ZIKV.



**Citation:** Loh, S.N.; Anthony, I.R.; Gavor, E.; Lim, X.S.; Kini, R.M.; Mok, Y.K.; Sivaraman, J. Recognition of *Aedes aegypti* Mosquito Saliva Protein LTRIN by the Human Receptor  $LT\beta R$  for Controlling the Immune Response. *Biology* **2024**, *13*, 42. <https://doi.org/10.3390/biology13010042>

Academic Editor: Yuxian He

Received: 3 December 2023

Revised: 4 January 2024

Accepted: 8 January 2024

Published: 12 January 2024

**Abstract:** Salivary proteins from mosquitoes have received significant attention lately due to their potential to develop therapeutic treatments or vaccines for mosquito-borne diseases. Here, we report the characterization of LTRIN (lymphotoxin beta receptor inhibitor), a salivary protein known to enhance the pathogenicity of ZIKV by interrupting the  $LT\beta R$ -initiated NF- $\kappa B$  signaling pathway and, therefore, diminish the immune responses. We demonstrated that the truncated C-terminal LTRIN ( $\Delta LTRIN$ ) is a dimeric protein with a stable alpha helix-dominant secondary structure, which possibly aids in withstanding the temperature fluctuations during blood-feeding events.  $\Delta LTRIN$  possesses two  $Ca^{2+}$  binding EF-hand domains, with the second EF-hand motif playing a more significant role in interacting with  $LT\beta R$ . Additionally, we mapped the primary binding regions of  $\Delta LTRIN$  on  $LT\beta R$  using hydrogen–deuterium exchange mass spectrometry (HDX-MS) and identified that <sup>91</sup>QEKAHIAEHMDVPIDTSKMSEQELQFHY<sup>118</sup> from the N-terminal of  $\Delta LTRIN$  is the major interacting region. Together, our studies provide insight into the recognition of LTRIN by  $LT\beta R$ . This finding may aid in a future therapeutic and transmission-blocking vaccine development against ZIKV.

**Keywords:** mosquito; saliva protein; Zika virus; human receptor; EF-hand



**Copyright:** © 2024 by the authors. Licensee MDPI, Basel, Switzerland. This article is an open access article distributed under the terms and conditions of the Creative Commons Attribution (CC BY) license (<https://creativecommons.org/licenses/by/4.0/>).

## 1. Introduction

Vector-borne diseases are caused by viruses, parasites and bacteria, and they are transmitted through vectors. These vectors can be insects, ticks, mites, fleas or even birds. According to the World Health Organization, vector-borne diseases account for 17% of all infectious diseases, leading to more than 700,000 deaths annually [1,2]. Mosquitoes

are known to be the most notorious vectors that spread infectious diseases to the public. Zika virus (ZIKV), dengue virus (DENV), chikungunya virus (CHIKV), yellow fever virus (YFV) and West Nile virus (WNV) are a few notorious viruses that use the mosquitoes as vectors to transmit infectious pathogens to humans through their bites [3,4]. This poses a significant threat to populations worldwide, especially in tropical and subtropical areas where mosquitoes thrive [2,5].

During an infected female mosquito blood-feeding, salivary proteins are injected into the human host along with the viruses. These salivary proteins are known to facilitate the blood-feeding event by impeding blood coagulation, platelet aggregation as well as vasoconstriction [4,6]. Recent studies have shown that some of these salivary proteins not only promote blood-feeding, but also enhance viral infection severity by hampering the human host's immune responses [4,6–8]. For instance, neutrophil-stimulating factor 1 (NeSt1), a 37 kDa protein found in *Aedes aegypti* mosquito saliva, enhances ZIKV pathogenesis by activating neutrophils, which further recruit virus-susceptible macrophages for ZIKV infection at the bite site [9,10].

Among these mosquito-borne diseases, the detection of ZIKV infection is relatively challenging because most infected individuals are asymptomatic. However, some of the ZIKV infected individuals may experience symptoms such as fever, muscle and joint pain, rashes and headaches [11,12]. These symptoms are common in other diseases such as DENV fever and CHIKV making correct identification of ZIKV infected individuals even more difficult. ZIKV is one of the few mosquito-borne diseases associated with neurological complications [13,14]. ZIKV infected adults have a higher risk of developing Guillain–Barré syndrome and radiculopathy [13]. Furthermore, ZIKV can be transmitted vertically from mother to fetus, which can lead to microcephaly and other severe neurological defects in newborns [3,11].

Despite the need for effective therapeutic treatment for ZIKV, no vaccine or drug is currently commercially available [11]. Previous studies have focused extensively on the development of a vaccine or a drug that directly targets the virus particle [15]. However, targeting the virus itself often leads to antibody-dependent enhancement, which in turn, facilitates the infection of other flaviviruses [16]. In recent years, researchers have shifted their focus from pathogen (virus)-centric interventions to vector (mosquito saliva)-centric interventions. The proof-of-concept for the effectiveness and safety of the saliva-centric approach has been demonstrated in the first ever *Anopheles* saliva protein vaccine human trials [17]. Furthermore, passive immunization of mice against mosquito salivary proteins has been shown as a promising alternative strategy for controlling the transmission of ZIKV and other vector-borne diseases [4,10,18].

In this study, we sought to characterize a salivary protein from *Aedes aegypti* named LTRIN (lymphotoxin  $\beta$  receptor inhibitor), which facilitates ZIKV transmission [19]. During a blood-feeding event, LTRIN is injected into the human host and interacts with the receptor  $LT\beta R$  (lymphotoxin  $\beta$  receptor).  $LT\beta R$  has two known binding partners:  $LT\alpha\beta$  heterotrimer and TNF superfamily member 14 (TNFSF14, also known as LIGHT). Upon binding with the ligand, the dimerization of  $LT\beta R$  is triggered and consequently activates both the canonical and non-canonical NF- $\kappa B$  pathways [19,20]. The activation of the NF- $\kappa B$  signaling pathways results in the synthesis of chemokine and cytokines, promoting the innate immune response [20]. Jin et al. showed that LTRIN binds to the N-terminal domain of  $LT\beta R$ , leading to inhibition of the NF- $\kappa B$  signaling pathway and subsequent production of pro-inflammatory cytokines [16]. Notably, mice that were pre-treated with anti-LTRIN before ZIKV infection survive better than those without treatment, suggesting LTRIN as a promising vaccination target to combat ZIKV infection [19].

Here, we report the characterization of  $\Delta$ LTRIN and its interaction with human  $LT\beta R$ , shedding light on its role in facilitating ZIKV transmission and infection. Through the application of hydrogen deuterium exchange mass spectrometry (HDX-MS) and site-directed mutagenesis, we successfully mapped the interacting interface between  $\Delta$ LTRIN and  $LT\beta R$ , while also identifying the specific amino acid residues within LTRIN that are

involved in these interactions. We additionally examined the secondary structure of LTRIN and assessed the influence of different divalent ions on it.

## 2. Materials and Methods

### 2.1. Maximum Likelihood Phylogenetic Tree

Similar protein sequences of LTRIN (XP\_011493643.1) and MCFD2 (CAD38756.1) were identified using the Protein BLAST tool [21]. Only proteins having fasta sequences with more than 70% similarity to *Insecta* and *Hominidae* were selected and combined for analysis. Sequence alignment and generation of maximum likelihood phylogenetic tree were performed using the program MEGA11 (Molecular Evolutionary Genetics Analysis version 11) with bootstrap value of 1000 [22].

### 2.2. Protein Expression and Purification

The full length LTRIN consists of a signal peptide and highly disordered region at its N-terminal. Only the residue from 86 to 210 was codon-optimized and cloned into a modified pET28a vector with an N-terminal 6-His tag followed by thrombin cleavage site. The vector was introduced into *E.coli* BL21 strain and was grown in LB media with 100 µg/mL of Amp<sup>+</sup> until the OD<sub>600</sub> reached 0.8. Then, 250 µM of isopropyl β-d-1-thiogalactopyranoside (IPTG) was added to the bacterial cell culture to induce the expression of ΔLTRIN, and the culture was allowed to continue to grow at 18 °C for 16 to 20 h.

The cell culture was pelleted at 3500 rpm for 30 min using a Beckman Coulter Centrifuge JLA-8.1 Rotor (Beckman Coulter, Brea, CA, USA). The purification procedures are described elsewhere [19]. Briefly, the pellets were washed once with PBS then resuspended in lysis buffer (50 mM Bis-Tris, 300 mM NaCl, 5% glycerol, 2 mM DTT pH 6.5). The cell was lysed using sonicator in the presence of 100 mM PMSF, cOmplete™ EDTA-free protease inhibitor cocktail (Thermo Fisher Scientific, Waltham, MA, USA) and 0.5% of Triton X100. The lysed product was centrifuged at 18,000 rpm using Beckmann Coulter Centrifuge JA-20 Rotor ((Beckman Coulter, Brea, CA, USA) for 30 min at 4 °C. The supernatant was subjected to Ni-NTA affinity chromatography followed by anion exchange chromatography to remove impurities. The His-tag was cleaved by incubating with thrombin at 4 °C overnight then further purified via size exclusion chromatography by using Superdex 75 column (GE HealthCare, Chicago, IL, USA). ΔLTRIN was kept in 50 mM Bis-Tris pH 6.5, 100 mM NaCl, 2% glycerol. The other mutants and constructs were purified using the same methods as the WT ΔLTRIN.

The extracellular domain of LTβR (residues Gln 31-Met 227) was expressed in Sf9 cell using Bac-to-Bac system according to manufacturer's recommendation (Invitrogen, Waltham, MA, USA). Briefly, the extracellular domain was first cloned into pFastBac HTB vector with gp67 signal peptide and 6-His tag addressed at the N-terminal. The sequence confirmed plasmid was transformed into DH10EmBacY competent cells and selected using blue-white screening. The recombinant bacmid DNA was extracted and transfected into Sf9 cells with CellFectin II transfection reagent (Invitrogen, Waltham, MA, USA). About 5–7 days following transfection, when cells exhibited visible cytopathic effect (>70%), the virus-containing supernatant was harvested as V<sub>0</sub> through centrifugation at 1000× g for 20 min. The V<sub>0</sub> baculovirus was subsequently utilized to infect Sf9 in order to produce V<sub>1</sub> as the baculovirus stock. High Five™ cells at a density of 2.0 × 10<sup>6</sup> cells/mL were infected by V<sub>1</sub> LTβR baculovirus at a concentration of 2–4% v/v for protein production. The infected cells were harvested at 60 h post-infection. The medium that contained secreted LTβR was subjected to Ni-NTA affinity chromatography and further purified using methods mentioned above. Similar method was used to prepare N40G N177G LTβR to remove N-linked glycosylation. Both LTβR and N40G N177G LTβR were stored in 50 mM Tris-HCl pH 7.5, 100 mM NaCl and 2% glycerol buffer.

### 2.3. Protein Refolding of LT $\beta$ R

The extracellular domain of LT $\beta$ R was cloned into a modified pET28a vector with 6-His tag and HRV 3C Protease cleavage site at the N-terminal. The protein was refolded following standard protocol described elsewhere [23]. Briefly, the cells were sonicated in 50 mM Tris-HCl pH 8.0, 300 mM NaCl, 2 M urea and 2% glycerol. The inclusion body was dissolved in 100 mM Tris-HCl, 8 M urea pH 8.0, then further purified using Ni-NTA column. The purified denatured protein sample was added dropwise into an agitating refolding buffer (100 mM Tris HCl, 2 mM EDTA, 400 mM L-arginine, 0.5 mM oxidized glutathione, 5 mM reduced glutathione, pH 8.0). The refolded protein was concentrated using Vivaspinn 20 centrifugal concentrator (Cytiva, Marlborough, MA, USA) with a molecular weight cutoff at 10 kDa. The concentrated protein was buffer exchanged to 50 mM Tris-HCl pH 7.5, 100 mM NaCl and 2% glycerol by using Superdex 75 column (GE HealthCare, Chicago, IL, USA).

### 2.4. Sedimentation Velocity-Analytical Ultracentrifugation of $\Delta$ LTRIN

The SV-AUC was carried out for  $\Delta$ LTRIN in 25 mM Tris HCl, 50 mM NaCl pH 7.5. The samples were examined by Beckman ProteomeLab XL-1 analytical ultracentrifuge (Beckman Coulter, Brea, CA, USA) equipped with an-60 Ti rotor. Next, 400  $\mu$ L of protein sample (0.5 mg/mL) was loaded into epon double-sector centerpieces equipped with quartz windows and centrifuged at 40,000 rpm, 20 °C in vacuum until full sedimentation. Then, 70 readings were obtained at A280 nm, with a 6-min interval between each reading. The scans from the 5th to the 50th scan were analyzed using SEDFIT16-1c software, employing the “Continuous c(s) distribution” model.

### 2.5. Dynamic Light Scattering of $\Delta$ LTRIN

The DLS measurements were performed to evaluate the homogeneity of  $\Delta$ LTRIN across different concentrations [24]. The DLS instrument was operated according to the manufacturer’s guidelines. Briefly, the  $\Delta$ LTRIN samples of different concentrations were centrifuged at 15,000 rpm for 10 min before measurement and then 4  $\mu$ L of the sample was added to the cuvette to perform measurement. All the scattered light intensity was measured using DynaPro Nanostar (Wyatt Technology, Santa Barbara, CA, USA).

### 2.6. Ruthenium Red Assay of $\Delta$ LTRIN

With BSA as negative control and MCFD2 as positive control, the purified  $\Delta$ LTRIN was subjected to electrophoresis on 15% SDS-PAGE gel. A total of 2  $\mu$ g of each protein sample was loaded into every well. The gel was then transferred onto PVDF membrane via Trans-Blot<sup>®</sup> Turbo<sup>™</sup> Transfer System (Bio-Rad, Hercules, CA, USA). The membrane was then washed with washing buffer (10 mM Tris-HCl, 60 mM KCl, 5 mM MgCl<sub>2</sub>, pH 7.5) 3 times and then stained with ruthenium red staining solution for 20 min at room temperature. The ruthenium red staining solution was prepared by dissolving ruthenium red in the washing buffer to a final working concentration of 25 mg/L [25].

### 2.7. Isothermal Titration Calorimetry of $\Delta$ LTRIN with Different Divalent Ions

The ITC measurements were conducted using MicroCal PEAQ-ITC (Malvern Panalytical, Malvern, UK). The protein samples were buffer exchanged to 50 mM Bis-Tris pH 6.5, 100 mM NaCl and concentrated to a series of concentrations ranging from 100  $\mu$ M to 300  $\mu$ M. The same buffer was used for preparing the ligands (CaCl<sub>2</sub>, MgCl<sub>2</sub>, ZnCl<sub>2</sub>) up to 5 mM. The measurement was carried out at 25 °C, with stirring speed at 500 rpm. Each injection was performed with a 2  $\mu$ L and 150 s spacing between injections. The data were analyzed using MicroCal PEAQ-ITC analysis software (version 1.40) with one set of sites fitting the model.

### 2.8. Gel Mobility Shift Assay of $\Delta$ LTRIN

The procedure for conducting the gel mobility assay was performed following the method described elsewhere [25]. Briefly, we prepared 15% SDS gel with 3 mM  $\text{Ca}^{2+}$  and 3 mM EDTA. Next, we prepared an equal amount of BSA (negative control), MCFD2 (positive control) and  $\Delta$ LTRIN in sample loading buffer, then loaded equal volume of all samples to both the SDS gel with 3 mM  $\text{Ca}^{2+}$  and 3 mM EDTA. The final quantity of 2  $\mu\text{g}$  of each protein sample was added to every well. The gel was visualized by Coomassie blue staining solution.

### 2.9. Circular Dichroism of $\Delta$ LTRIN and its Mutants

Around 0.3 mg/mL of  $\Delta$ LTRIN, D123A, D180A and D123A D180A mutants were prepared in 5 mM Tris-HCl, 25 mM NaCl pH 7.5 buffer. The samples were centrifuged at 15,000 rpm, 4 °C before loading into the cuvette. Subsequently, 200  $\mu\text{L}$  of centrifuged protein sample with final concentration of 2 mM of EGTA or 5 mM of  $\text{CaCl}_2$  was loaded into the cuvette. Washes were conducted after each measurement. The far UV Circular Dichroism (FUV-CD) spectroscopy was measured using J-1100 Circular Dichroism spectrometer (Jasco Inc., Tokyo, Japan). The CD spectra profile of  $\Delta$ LTRIN as a function of temperature was also obtained by measuring at 222 nm across 20 to 100 °C.

### 2.10. ELISA

The ELISA assay was conducted according to Thermo Fisher Scientific's (Waltham, MA, USA) protocol. Briefly, 10  $\mu\text{g}$  of  $\Delta$ LTRIN or FL LTRIN or  $^{119}\text{LTRIN}^{210}$  was coated on each well of 96-well flat bottom plate overnight at 4 °C. After incubating with 5% of BSA blocking buffer in PBST for 2 h at 37 °C, 0.15  $\mu\text{g}$  of WT LT $\beta$ R, refold LT $\beta$ R and LT $\beta$ R N40G N177G were added to each well and incubated at room temperature for another 2 h. Rabbit monoclonal against LTBR (80178-T16, Sino Biological, Beijing, China) and anti-rabbit IgG conjugated with HRP (A120-101P, Bethyl Laboratories, Montgomery, AL, USA) were used as primary and secondary antibodies, respectively. TMB-ELISA substrate (3,3',5,5'-Tetramethylbenzidine) was added for color development and was measured at 450 nm using plate reader (Infinite<sup>®</sup> M Nano+, Tecan, Männedorf, Switzerland).

### 2.11. Hydrogen-Deuterium Exchange Mass Spectrometry

In this experiment, 90 pmol of  $\Delta$ LTRIN and LT $\beta$ R proteins was used for each HDX experiment (apo  $\Delta$ LTRIN, or  $\Delta$ LTRIN and LT $\beta$ R complexes) from stock solution containing 1 mg/mL  $\Delta$ LTRIN and 2 mg/mL LT $\beta$ R.

Deuterium exchange buffer was prepared by drying aqueous PBS buffer pH 7.4 to remove all  $\text{H}_2\text{O}$ , and 99.9%  $\text{D}_2\text{O}$  was added to reconstitute to form the deuterium exchange buffer. Amide hydrogen deuterium exchange reaction was initiated by adding apo  $\Delta$ LTRIN, or  $\Delta$ LTRIN and LT $\beta$ R complexes into 10 $\times$  volume of deuterium exchange buffer to yield a final  $\text{D}_2\text{O}$  concentration of 89.9%. Deuterium labelling was then carried out at 2 different deuterium exposure times of 1 min and 100 min.

HDX reaction was quenched by reducing pH of the reaction to 2.5 by adding formic acid in GnHCl to achieve a final concentration of 1.5 M GnHCl. Quenching of reaction was performed for 1 min on ice to further slowdown any back exchange reaction. All deuterium exchange reactions were performed in triplicate and the final deuterons uptake value for each peptic digested fragment reported is an average value of the triplicates without back exchange correction.

All quenched samples were injected into nano-UPLC HDX sample manager (Waters, Milford, MA, USA), online pepsin digestion was performed using a Waters Enzymate BEH pepsin (2.1  $\times$  30 mm) column in 0.05% formic acid in water at 100 mL/min. Proteolyzed pepsin fragment peptides were trapped by a 2.1  $\times$  5 mm C18 trap (ACQUITY BEH C18 VanGuard Pre-column, 1.7 mm, Waters, Milford, MA, USA) and eluted with an 8–40% gradient of acetonitrile in 0.1% formic acid at 40 mL/min into a reverse phase column (ACQUITY UPLC BEH C18 Column, 1.0  $\times$  100 mm, 1.7 mm, Waters) by nano ACQUITY

Binary Solvent Manager (Waters, Milford, MA, USA). Peptides were ionized by electrospray into SYNAPT G2-Si mass spectrometer (Waters, Milford, MA, USA) acquiring in MSE mode for detection and mass measurements. Next, 200 fmol/mL of [Glu1]-fibrinopeptide B ([Glu1]-Fib) was simultaneously injected into the mass spectrometer at a flow rate of 10 mL/min for continuous calibration during sample acquisition [26].

All deuterium uptake calculations were performed using DYNAMX 3.0 software (Waters, Milford, MA, USA). Deuteron uptake per peptide was obtained by subtracting mass centroid of deuterium exposed peptides (1 min and 100 min) with the mass centroid of the undeuterated peptide. Differences between  $\Delta$ LTRIN and LT $\beta$ R complex with  $\Delta$ LTRIN apo state were then obtained by subtracting deuterons uptake of all peptides in the  $\Delta$ LTRIN and LT $\beta$ R complex with  $\Delta$ LTRIN apo state and represented as a difference plot of peptides spanning from N to C terminus.

### 3. Results

#### 3.1. Evolutionary Relationship of LTRIN with Insecta and Hominoidea

Maximum likelihood phylogenetic tree was created to illustrate a hypothesized evolutionary path of mosquito salivary protein LTRIN from *Aedes aegypti* (XP\_011493643.1) with closely related proteins. Through a BLASTp analysis, we observed that multiple coagulation factor deficiency protein 2 (MCFD2) of *Aedes aegypti* (XP\_021693757.1), *Aedes albopictus* (XP\_019530660.2) and *Anopheles stephensi* (XP\_035902781.1) *Insecta* share a sequence identity of 99.05%, 67.18% and 77.78% to LTRIN, respectively. The main function of MCFD2 in *Homo sapiens* is to shuttle various metabolic proteins between the endoplasmic reticulum (ER) and the ER-Golgi intermediate compartment during blood clotting [27]. LTRIN of *Aedes aegypti* and MCFD2 of *Homo sapiens* (AAP23162.1) share a 41.94% sequence identity, and is mainly contributed by the presence of EF-hand motif. Further examination of the evolutionary relationship of these homolog proteins was performed together with these proteins' respective superfamilies. Thus, MCFD2 protein of *Homo sapiens* was also subjected to a BLASTp. Results from both BLASTp were collated and aligned to create a maximum likelihood phylogenetic tree (Figure 1a). The phylogenetic tree shows a good confidence value as all bootstrap values are over 60% and six out of the eleven values are over 90%. *Insecta* and *Hominoidea* distinctively split into branches with lengths of 0.3 and 1.0, respectively, which reveal greater genetic and functional change in *Hominoidea* than *Insecta* when compared with the ancestral state. LTRIN has a shorter branch length of 0.5, as compared to the 1.0 of *Homo sapiens* MCFD2. In humans, MCFD2 is involved in transport of FV and FVIII from ER to Golgi [27]. To understand the mode of recognition of receptor LT $\beta$ R and LTRIN, in the following sections we present the characterization of LTRIN and its interactions with the receptor.

#### 3.2. LTRIN Exists as a Dimer

The full-length LTRIN is 22 kDa with a signal peptide and a highly disordered region at the N terminal. It was reported that the 15 kDa C-terminal region of LTRIN alone is sufficient to interact with LT $\beta$ R [19]. Hence, the 15 kDa truncated C-terminal <sup>86</sup>LTRIN<sup>210</sup> (hereafter referred as  $\Delta$ LTRIN) is expressed in *E. coli* bacterial cells (Figure 2a). The protein is purified using size exclusion chromatography after passing through Ni-NTA affinity chromatography. The elution profile shows that  $\Delta$ LTRIN is eluted as a dimer with a molecular weight of around 30 kDa (Figure 2b). The dimerization of  $\Delta$ LTRIN is further confirmed using sedimentation velocity-analytical ultracentrifugation (SV-AUC) sedimentation velocity (Supplementary Figure S1a). The  $\Delta$ LTRIN has a size distribution at 30.6 kDa, supporting its dimerization.

Occasionally, protein oligomerization is triggered by high protein concentrations or interactions between proteins and ions [28–30]. To elucidate whether the oligomerization state of  $\Delta$ LTRIN is driven by concentration or not, dynamic light scattering (DLS), as well as static light scattering (SLS) of different concentrations of  $\Delta$ LTRIN, ranging from 1 mg/mL to 20 mg/mL, were measured. Supplementary Figure S1b shows that the dimerization of  $\Delta$ LTRIN remains relatively stable across the various concentrations measured, as evidenced

by the consistent and narrow peak in the DLS profile. Similarly, there was no effect on the dimerization state of  $\Delta$ LTRIN in the presence of  $\text{Ca}^{2+}$  or EDTA, indicating that interactions with ions do not play a role in  $\Delta$ LTRIN dimerization (Supplementary Figure S1c,d).

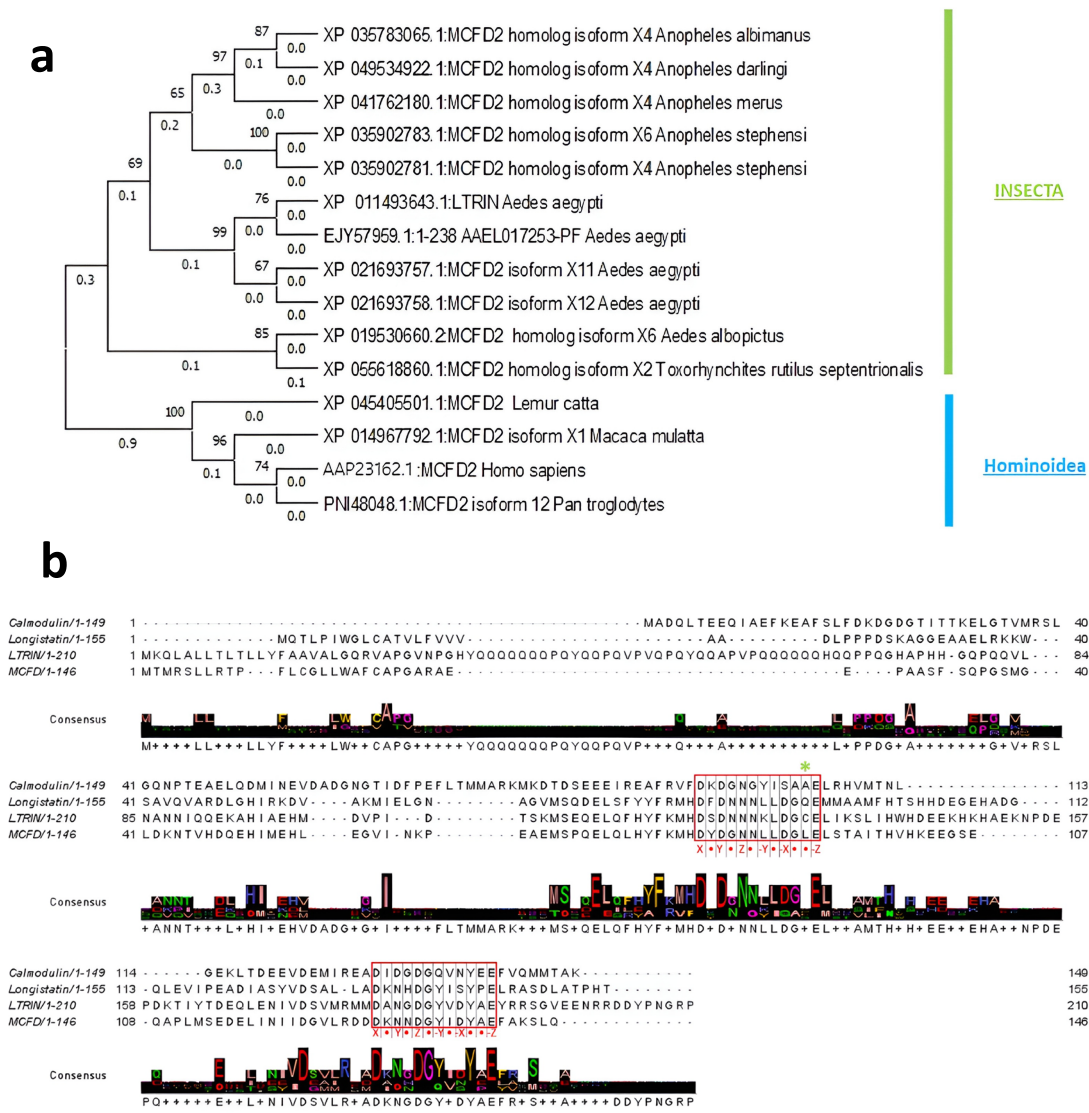


**Figure 1.** (a) Maximum likelihood phylogenetic tree of mosquito salivary protein LTRIN from *Aedes Aegypti* (XP\_011493643.1) and multiple coagulation factor deficiency protein 2 (MCFD2) from insect and human. (b) Sequence alignment of LTRIN with human MCFD2 and calmodulin. The EF-hand motif is highlighted using a red box. The  $\text{Ca}^{2+}$  binding loop sequence is highly conserved among all three proteins, arranging in X • Y • Z • -Y • -X • • -Z fashion, where X and -Z are usually occupied by Asp and Glu. The C133 position of LTRIN is denoted with \*.

The sulfhydryl group or thiol group (S-H) of cysteine can form a disulfide bond (S-S) with another cysteine residue. These bonds are known to play a crucial role in protein folding and stabilization as well as cysteine-mediated oligomerization [31,32].  $\Delta$ LTRIN consists of a cysteine residue located at position 133, which can potentially form a disulfide bond with the cysteine residue from another molecule, and could form the dimers. SDS-PAGE was conducted with and without the addition of reducing agent ( $\beta$ -mercaptoethanol). In the absence of the reducing agent, a small portion appeared in dimer form (band around 35 kDa), while most of the  $\Delta$ LTRIN was observed in its monomeric state (band at 15 kDa) (Figure 2c), suggesting that disulfide bond formation is not the primary cause of  $\Delta$ LTRIN dimerization. We further introduce a point mutation at position 133 to make C133Q/L variant taking clues

for the sequence alignment with its insect homolog longistatin and human homolog MCFD2 (Figure 1b) [33]. The size exclusion chromatography elution profile of C133Q/L indicates that it still forms a dimer and is further confirmed by DLS (Supplementary Figure S1e,f). This suggests that the dimerization is not mediated by the disulfide bonds, but it could be facilitated by electrostatic interactions involving the charged residues found in LTRIN [34].

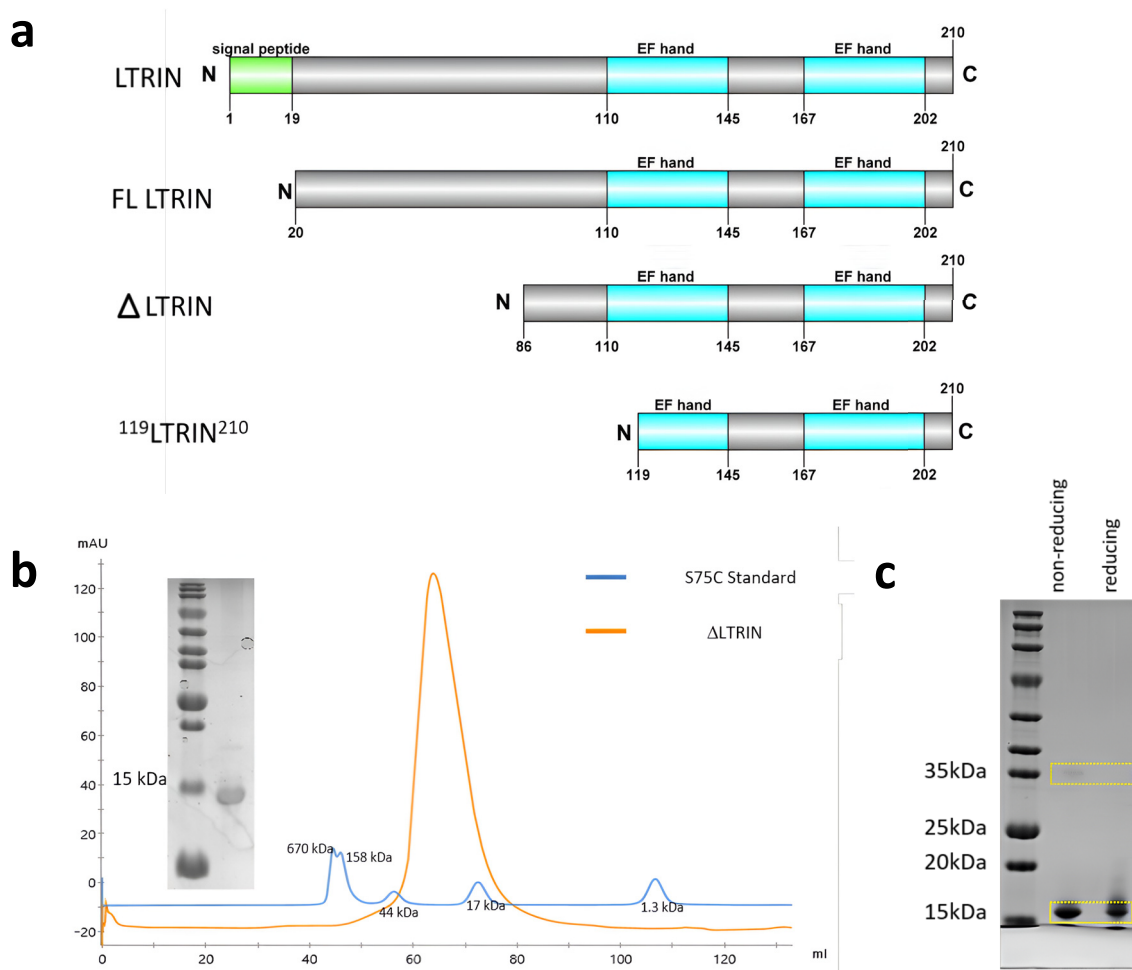


**Figure 2.** (a) The full length of LTRIN consists of signal peptide and two calcium-binding EF-hand domains. (b) ΔLTRIN size exclusion chromatography elution profile after Ni-NTA affinity column and ion exchanger chromatography. The blue line represents the standard curve, indicating that ΔLTRIN (orange) eluted between 44 kDa and 17 kDa, which implies the formation of a dimer. (c) SDS PAGE with and without reducing agent (β-mercaptoethanol) was conducted to analyze the dimerization of ΔLTRIN. In the presence of the reducing agent, most of ΔLTRIN was observed in its monomeric state, indicating that disulfide bond formation is not the main factor contributing to ΔLTRIN's dimerization. ΔLTRIN is highlighted with a yellow box.

### 3.3. LTRIN Has EF-Hand Motifs and Binds to Ca<sup>2+</sup> and Other Divalent Ions

The EF-hand motif is characterized by a helix-loop-helix secondary structure with two α-helices connected by a Ca<sup>2+</sup> binding loop. This binding loop consists of 12 amino acids and is typically structured in the fashion of X • Y • Z • -Y • -X • • -Z, where X, Y, Z, -Y, -X, -Z denote the amino acids that coordinate with Ca<sup>2+</sup> ions and • represents the intervening residues. The X and -Z positions are highly conserved, and are usually occupied by Asp and Glu, respectively. Asp or Asn is commonly found at position Y, whereas positions Z and -X can be occupied by either Asp, Asn, or Ser. The -Y position is rather flexible; many different residues have been observed [35–38]. Examining the protein sequence of LTRIN, we observed two sets of potential EF-hand motifs with the Ca<sup>2+</sup> binding loop sequence as

follows: <sup>123</sup>DSDNNKLDGCE<sup>134</sup> and <sup>180</sup>DANGDGYVDYAE<sup>191</sup>. These loop sequences are highly negatively charged with Asp and Glu at position X and -Z, respectively, and these sequences are highly conserved among other EF-hand domain proteins (Figure 1b).

Ruthenium red is a polycationic stain that has been used to identify proteins with EF-hand motif [25,39]. We performed ruthenium red staining using MCFD2 as a positive control. We found that  $\Delta$ LRIN binds to ruthenium red and confirmed the presence of EF-hand motif (Supplementary Figure S2a). Further, the Ca<sup>2+</sup> binding ability of  $\Delta$ LRIN is confirmed by isothermal titration calorimetry (ITC) with K<sub>D</sub> value  $27.3 \times 10^{-6} \pm 9.43 \times 10^{-6}$  M (Supplementary Figure S2c). The Ca<sup>2+</sup> binding EF-hand motif is also known to accommodate other divalent ions such as Mg<sup>2+</sup> and Zn<sup>2+</sup> [40,41]. We also performed ITC experiments with these two ions. Interestingly,  $\Delta$ LRIN does not interact with Mg<sup>2+</sup> and has lower binding affinity with Zn<sup>2+</sup> compared to Ca<sup>2+</sup> (Supplementary Figure S2c).

In some cases, the binding of Ca<sup>2+</sup> to EF-hand motif can lead to significant conformational changes. In order to examine the possible conformational changes of  $\Delta$ LRIN upon binding with Ca<sup>2+</sup>, gel mobility shift assay has been carried out [25]. Supplementary Figure S2b shows that the presence of Ca<sup>2+</sup> did not significantly alter the mobility of  $\Delta$ LRIN, indicating that binding with Ca<sup>2+</sup> does not result in a significant conformational change in it. This conclusion is also supported by Circular Dichroism (CD) studies (discussed below).

### 3.4. LRIN Has a Stable Alpha-Helix Dominant Structure over a Wide Range of Temperatures

The secondary structure of  $\Delta$ LRIN was analyzed using CD (Figures 3b and S1g). The results showed two negative peaks detected at approximately 222 nm and 208 nm, implying that  $\Delta$ LRIN has an  $\alpha$ -helix dominant secondary structure, and such observations are consistent with the predicted secondary structure (Figures 3a and S1h) [42]. Further, the CD spectra of  $\Delta$ LRIN were used to estimate its secondary structures through three different methods (SELCON3, CONTINLL and CDSSTR), and subsequently compared with the structure predicted by AlphaFold [43]. Both experimental and computational analyses were consistent, which showed that  $\Delta$ LRIN possesses mainly alpha-helix and loop structures (Supplementary Table S1).

In contrast to MCFD2,  $\Delta$ LRIN possesses a well folded secondary structure even in the absence of Ca<sup>2+</sup>. Regardless, adding Ca<sup>2+</sup> did not alter the overall secondary structure of  $\Delta$ LRIN; instead, it undergoes more subtle structural changes as evidenced by the similar but deeper spectral patterns observed in both the absence and presence of Ca<sup>2+</sup> (Figure 3b). This observation is consistent with the gel mobility assay results (Supplementary Figure S2b).

Thermostability is an important feature of protein to maintain its secondary structure and perform its activity effectively. We investigated the conformational changes of  $\Delta$ LRIN at various temperatures. The CD data show that  $\Delta$ LRIN has a relatively stable secondary structure across a wide range of temperatures. Even heating up to 100 °C,  $\Delta$ LRIN did not completely lose its secondary structure; instead, it only underwent partial denaturation and indicated that LRIN is highly thermostable (Figure 3c,d).

### 3.5. Disulfide Bonds in LT $\beta$ R

LT $\beta$ R, a type-I transmembrane glycoprotein, belongs to the tumor necrosis factor (TNF) superfamily. Its extracellular domain consists of four cysteine-rich domains (CRD1–CRD4), which are responsible for the recognition of other TNF ligands. Each domain is approximately 40–44 amino acid residues in length. CRD1–3 consists of six Cys residues, forming three intradomain disulfide bonds within each domain, while CRD4 has four Cys residues, forming two disulfide bonds (Cys170–Cys185 and Cys191–Cys210). N-linked glycosylation sites are present at positions Asn40 and Asn177 of LT $\beta$ R [20,44]. We have expressed this protein using baculovirus expression system, and it is secreted with glycosylation (Figure 4b).

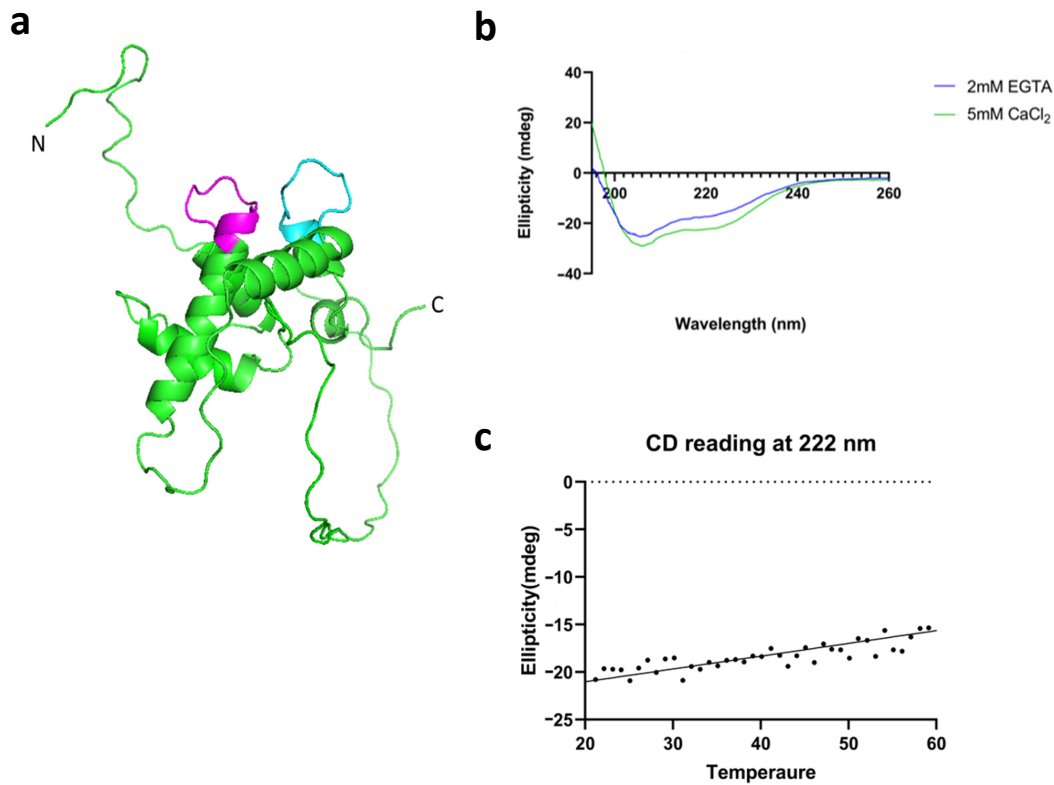


**Figure 3.** (a) The full length LTRIN structure modelled using AlphaFold. The N-terminal is showing random coiling. The Ca<sup>2+</sup> binding loops are highlighted in magenta (the first binding loop) and cyan (the second binding loop). (b) Circular dichroism (CD) spectra of ΔLTRIN in presence of CaCl<sub>2</sub> and EGTA. ΔLTRIN preserved its α-helix dominant secondary structure with or without the presence of Ca<sup>2+</sup>. (c) CD spectra reading of ΔLTRIN at 222 nm from 20 °C to 60 °C showing that ΔLTRIN has high thermostability.

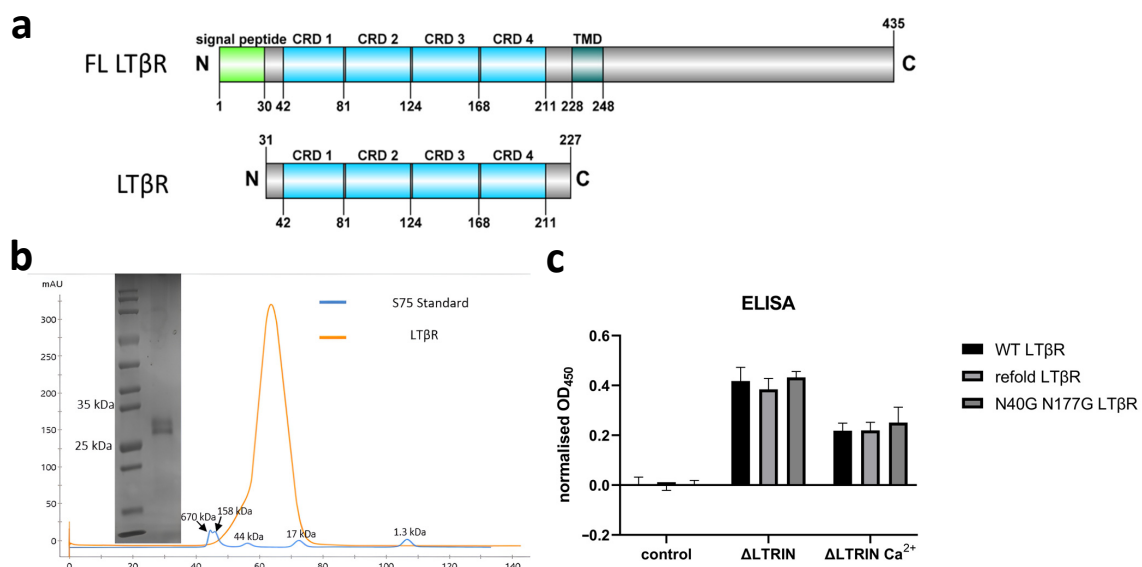


**Figure 4.** (a) Full length LTRβR is a transmembrane protein with signal peptide at N-terminal. The extracellular domain is used for the study. (b) The cysteine rich extracellular domain (CRD) of LTRβR expressed in insect High Five™ cell line via baculovirus expression system. The blue line indicates the standard curve, demonstrating that LTRβR (orange) possesses a molecular weight ranging from 44 kDa to 17 kDa. (c) ΔLTRIN interacts with LTRβR and the interaction is not dependent on either divalent ions or glycosylation. TMD: transmembrane domain.

### 3.6. The Interactions between LTRIN and $LT\beta R$ Are Not Affected by the Glycosylation of $LT\beta R$ or Divalent Ions

ELISA binding experiments were conducted to investigate the binding between  $\Delta LTRIN$  and  $LT\beta R$ . Our experiments showed that the binding between  $\Delta LTRIN$  and extracellular domain of  $LT\beta R$  was independent of the presence of divalent  $Ca^{2+}$  ions (Figure 4c). It is well known that the metal ion  $Zn^{2+}$  is widely used to precipitate proteins [45]. In our case, the excessive amount of  $Zn^{2+}$  also caused  $\Delta LTRIN$  precipitation and it could explain the negative value in ELISA binding (Supplementary Figure S2d). Although  $\Delta LTRIN$  consists of canonical EF-hand motif that binds to  $Ca^{2+}$ , our results showed that it does not require the divalent ions to interact with  $LT\beta R$ . In fact, the binding is slightly impeded in the presence of metal ion (Figure 4c).

Glycosylation is known to play an important role in regulating cell functions including intercellular communication and intracellular signaling pathways [46–48]. In order to examine the effect of  $LT\beta R$  glycan in  $\Delta LTRIN$  interactions, point mutations at these two glycosylation sites (N40G N177G  $LT\beta R$ ) were generated. The data show that N40G N177G  $LT\beta R$  has similar binding affinity toward  $\Delta LTRIN$  compared to WT  $LT\beta R$ , indicating that the interaction between  $LT\beta R$  and LTRIN is independent of the glycosylation of  $LT\beta R$  (Figure 4c).

### 3.7. Mapping the Interaction Sites of $\Delta LTRIN$ with $LT\beta R$

HDX-MS is performed to determine the interaction site of  $\Delta LTRIN$  with  $LT\beta R$ . Interestingly, the HDX-MS result revealed that the N-terminal of LTRIN ( $^{91}QEKAHIAEHMDVPIDT-SKMSEQELQFH Y^{118}$ ) is playing the key role in interacting with  $LT\beta R$  (Figure 5a).

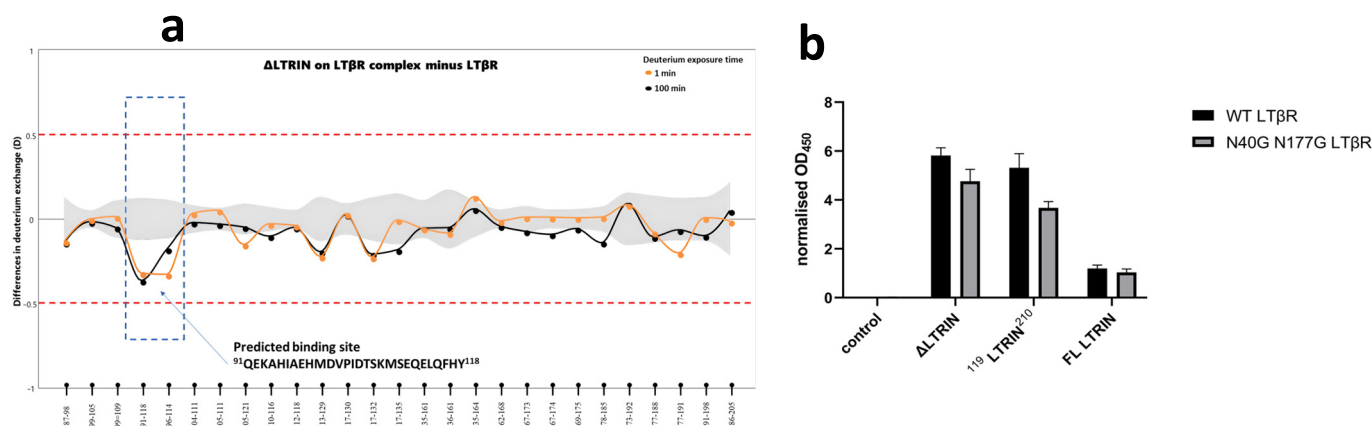


**Figure 5.** The interacting site of  $\Delta LTRIN$  on  $LT\beta R$ . (a) Plot depicting differences in deuterium exchange (Y-axis) between apo and bound form of  $\Delta LTRIN$ . The interacting peptide sequence is proposed to be  $^{91}QEKAHIAEHMDVPIDTSKMSEQELQFHY^{118}$ . (b) The ELISA shows both FL LTRIN and truncated  $^{119}LTRIN^{210}$  in binding.

According to the predicted structure using both AlphaFold and PSIPRED, the N-terminal of LTRIN including the proposed interacting region displays as random coil structure followed by a helix–loop–short helix–loop structure before entering the E-helix of the first EF-hand motif (Figures 3a and S1h). The HDX-MS data suggested that this helix–loop–short helix–loop structure together with the N-terminal of the E-helix of the first EF-hand are responsible for the interaction with  $LT\beta R$ . It would be intriguing to investigate the interaction between full-length LTRIN and  $LT\beta R$ , as well as determine whether the random coil N-terminal region plays a role in this interaction within the context of the full-length protein. To validate the involvement of the N-terminal interacting site, we expressed another two constructs termed  $^{119}LTRIN^{210}$  by deleting the interacting segment suggested by HDX-MS data and also the full length of LTRIN (hereafter referred as FL LTRIN without the signal peptide).

ELISA was carried out using both the FL LTRIN and the construct  $^{119}\text{LTRIN}^{210}$  (Figure 5b). The binding affinity between the FL LTRIN and  $\text{LT}\beta\text{R}$  is significantly reduced while that of  $^{119}\text{LTRIN}^{210}$  shows a slight reduction in binding when compared to the  $\Delta\text{LTRIN}$ .

### 3.8. The Second EF-Hand of $\Delta\text{LTRIN}$ Plays an Important Role in Interacting with $\text{LT}\beta\text{R}$

Despite the fact that the presence of  $\text{Ca}^{2+}$  does not affect the secondary structure of  $\Delta\text{LTRIN}$ , modifications were implemented on its EF-hands to assess how its interaction with  $\text{LT}\beta\text{R}$  would be affected by its binding ability with calcium. D123A, D180A and D123A D180A mutants were made to disrupt the calcium-binding ability of either the first or second or both EF-hands in  $\Delta\text{LTRIN}$ . The secondary structures of all the mutants were examined using CD and compared to wild-type  $\Delta\text{LTRIN}$ . Figure 6a shows that the  $\alpha$  helix-dominated secondary structure of  $\Delta\text{LTRIN}$  was well preserved in all the mutants in the presence of either  $\text{Ca}^{2+}$  or EDTA, further indicating that disruption of calcium binding in the EF-hands did not affect the overall secondary structure of  $\Delta\text{LTRIN}$ .

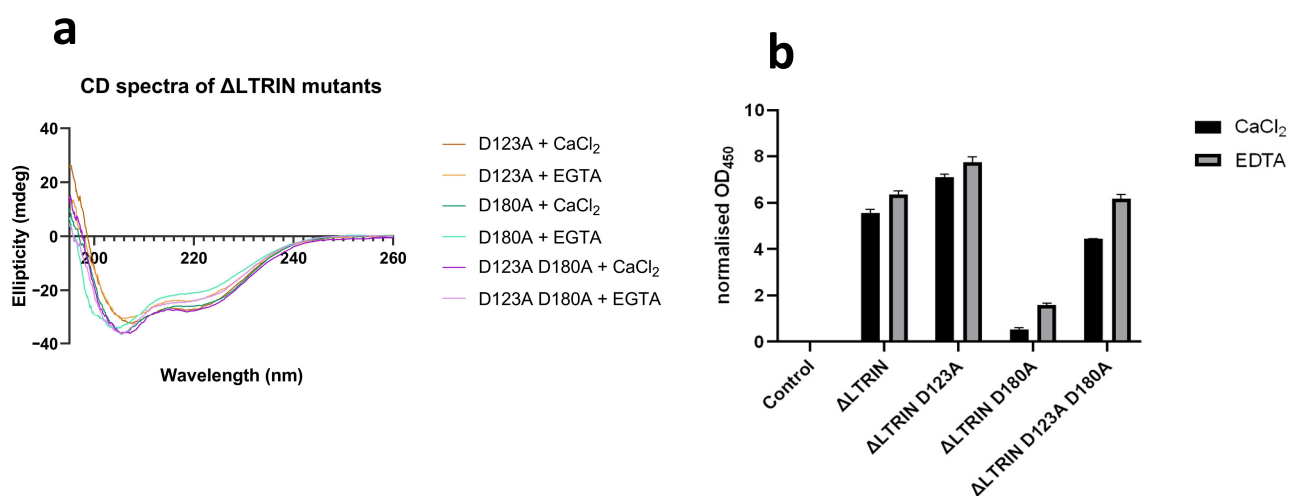


**Figure 6.** Altering the calcium-binding loop of EF-hands in  $\Delta\text{LTRIN}$ . (a) The secondary structure of  $\Delta\text{LTRIN}$  remains unchanged regardless of the ability to bind calcium or the presence of  $\text{Ca}^{2+}$ . (b) The ELISA results indicate that mutating D123A enhances interaction, while mutating D180A disrupts the interaction between  $\Delta\text{LTRIN}$  and  $\text{LT}\beta\text{R}$ .

ELISA was conducted on all the mutants, and it was observed from the results that the D123A mutation, which impaired the calcium-binding capability of the first EF-hand motif, did not decrease but rather slightly enhanced the interaction between  $\Delta\text{LTRIN}$  and  $\text{LT}\beta\text{R}$ . However, the D180A mutant, which disrupted the calcium-binding ability of the second EF-hand motif in  $\Delta\text{LTRIN}$ , exhibited a significant reduction in  $\Delta\text{LTRIN}$  interaction with  $\text{LT}\beta\text{R}$ . This suggests that the second EF-hand of  $\Delta\text{LTRIN}$  plays an important role in interacting with  $\text{LT}\beta\text{R}$ . Notably, the interaction between  $\Delta\text{LTRIN}$  and  $\text{LT}\beta\text{R}$  was not completely abolished by the double mutant D123A D180A. In fact, the interaction was restored to a level similar to that of the wild-type  $\Delta\text{LTRIN}$ , suggesting the D123A mutation favors the interaction (Figure 6b).

These findings indicate that calcium-binding capability of both EF-hands contributes to the interaction between  $\Delta\text{LTRIN}$  and  $\text{LT}\beta\text{R}$ , with the second EF-hand motif playing a more crucial role.

## 4. Discussion

The maximum likelihood phylogenetic tree shows that LTRIN and MCFD2 share the same origin. We assessed the protein sequence and the predicted secondary structure of both LTRIN and MCFD2 and showed that they are highly similar. Therefore, we speculate that MCFD2 will likely interact with  $\text{LT}\beta\text{R}$  due to its high sequence similarity and the

presence of EF-hand motif. As *Hominoidea* show a greater genetic and functional change than *Insecta* when compared to the ancestral state, LTRIN has closer relations to the ancestral state than *Homo sapiens* MCFD2, which might be the reason for LTβRs' preferential binding of LTRIN.

EF-hands motif is known to bind with Ca<sup>2+</sup> and sometimes the binding will give rise to conformational change [49–51]. MCFD2 has a random coiled secondary structure as an apo protein. Its C-terminal undergoes conformational changes to form the canonical helix-loop-helix structure upon interaction with Ca<sup>2+</sup> [52,53]. Although the majority of EF-hand proteins undergo conformational changes upon binding with Ca<sup>2+</sup>, some proteins maintain the same secondary structure even in the presence of Ca<sup>2+</sup> [54,55]. As suggested by our data, ΔLTRIN holds a well folded conformation in apo form and the presence of Ca<sup>2+</sup> ion has limited effect on its secondary structure. This is further supported by the observation that eliminating the ability of EF-hand motifs of ΔLTRIN to bind calcium ions did not cause significant alterations in its secondary structure.

Our data shows that ΔLTRIN forms a homodimer regardless of the protein concentration or the presence of Ca<sup>2+</sup>, and this is not contributed through the formation of disulfide bond. We suggest that the dimerization is through hydrophobic and electrostatic interaction between the EF-hand motifs of ΔLTRIN [56]. This implies that the Ca<sup>2+</sup>-binding domain can also serve as a dimerization unit. In fact, a few of the EF-hand Ca<sup>2+</sup>-binding proteins are reported to form dimers through hydrophobic interactions between the EF-hand motifs [57].

Oligomerization in EF-hand domain proteins is commonly observed as it provides extra interacting sites. Activation of the NF-κB signaling pathway is through dimerization of LTβR. Jin et al., reported that LTRIN disrupts the dimerization of LTβR; hence, diminishing the signaling pathway [19]. We speculate that homodimer of ΔLTRIN will interact with two adjacent LTβR forming a heterotetramer, resulting in the prevention of LTβR dimerization.

Blood-taking is a very stressful event for a mosquito as it requires dealing with abrupt temperature changes, from 22 to 37 °C [58]. Similarly, the salivary protein that is injected into the human host needs to have high thermostability to withstand the host body temperature and maintain its function. The temperature-dependent CD shows that LTRIN can preserve its structure regardless of the temperature.

According to the ELISA result, the binding affinity of LTβR, N40G, N177G LTβR and refolded LTβR with ΔLTRIN suggests that the interaction is not dependent on post translational modifications of LTβR. Interestingly, the presence of Ca<sup>2+</sup> ions slightly disrupt the interaction. We hypothesize that this could be due to the subtle conformational change in ΔLTRIN induced by the ions. As indicated by the CD data, the interaction of ΔLTRIN with Ca<sup>2+</sup> ion leads to a more compact and well-folded structure, leading to decreased flexibility and subsequently reduced binding affinity.

From the result of HDX-MS, it was identified that the N-terminal region of ΔLTRIN is responsible for interacting with LTβR. However, the FL LTRIN which composes the interacting site showed a great reduction in binding with LTβR. The N-terminal region of the full-length LTRIN is predicted to be a 65-amino acid-long segment that lacks defined structure and adopts a random coil conformation. We hypothesized that this flexible random coil may adopt certain conformations which hinder its ability to interact with LTβR, resulting in reduced binding affinity. This also explains why only the ΔLTRIN, rather than the intact full-length protein, is found in mosquitoes' saliva [19]. The randomly coiled portion needs to be removed through cleavage in order for the interaction site to become exposed and allow binding with LTβR, and subsequently, inhibit the NF-κB signaling pathway. Future studies are necessary to validate the role of the N-terminal region of FL LTRIN in mediating the interaction with LTβR.

The removal of the interacting site from <sup>119</sup>LTRIN<sup>210</sup> did not completely abolish its binding with LTβR but only resulted in a slight decrease. This observation can be explained by two hypotheses. Firstly, the construct <sup>119</sup>LTRIN<sup>210</sup> may retain the binding affinity due to other residues or regions within the protein that are able to compensate for the loss of the interacting site. This compensatory mechanism is sometimes seen in other

protein interactions, where other binding sites or alternative residues can contribute to the interaction when the primary binding site is not available [59]. This can be further explained by the notable decrease in interaction between D180A and LT $\beta$ R, indicating that the involvement of the second EF-hand motif in  $\Delta$ LTRIN in binding to LT $\beta$ R plays a role. However, the fact that the double mutant D123A D180A restored the interaction to wild-type levels suggests that the D123A mutation may enhance the interaction with LT $\beta$ R. Overall, these findings highlight the complex nature of the interaction between  $\Delta$ LTRIN and LT $\beta$ R, involving multiple residues and regions within  $\Delta$ LTRIN that contribute to binding affinity. Secondly, similar to what was observed with FL LTRIN, the shorter random coil N-terminal of  $\Delta$ LTRIN could still affect the interaction as well. In particular, removing residues from 91 to 118 exposes more of the hindered interacting site and facilitates its binding with LT $\beta$ R [60].

## 5. Conclusions

In summary, we demonstrate that  $\Delta$ LTRIN exists as a homodimer. Despite being an EF-hand protein, its secondary structure is not affected by binding to Ca<sup>2+</sup>. Through ELISA assay and HDX-MS, we identified the binding region of  $\Delta$ LTRIN with LT $\beta$ R. Although the presence of Ca<sup>2+</sup> does not affect the binding affinity, disrupting the calcium-binding ability specifically in the second EF-hand motif significantly affects the interaction between  $\Delta$ LTRIN and LT $\beta$ R (Figure 7). The decrease in binding affinity of FL LTRIN explains the reason behind the presence of only the truncated form,  $\Delta$ LTRIN, in the saliva of mosquitoes as the N-terminal region hinders its interaction. Our findings provide mechanistic insight into the interactions between LTRIN and LT $\beta$ R, which will aid in the development of inhibitors against  $\Delta$ LTRIN as a potential treatment or vaccine target for ZIKV. Understanding the binding mechanism of LTRIN with LT $\beta$ R sheds light on how specific regions play a role in mediating this interaction.

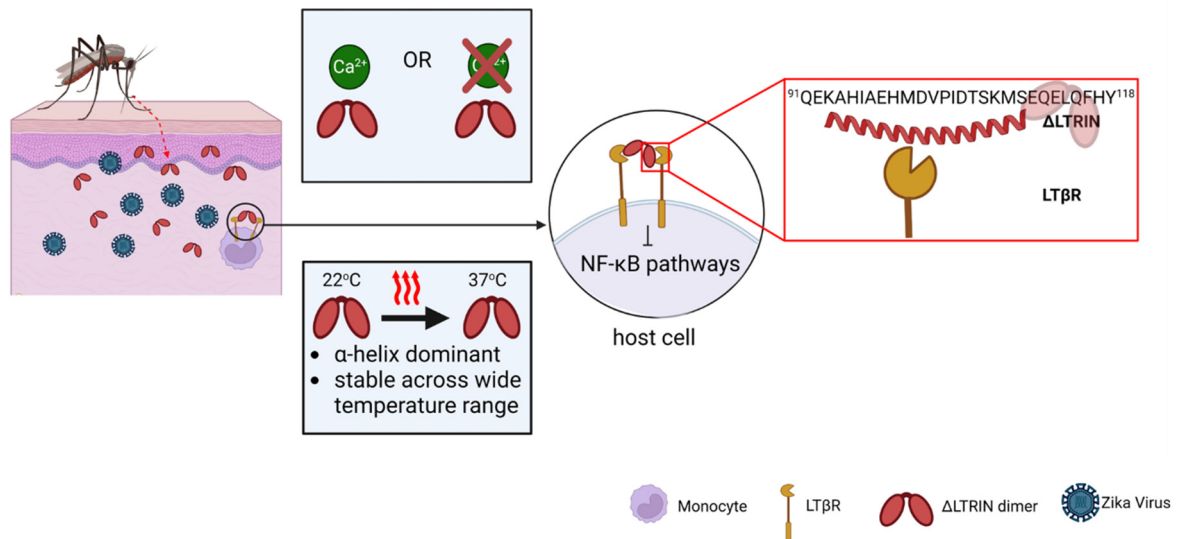


**Figure 7.**  $\Delta$ LTRIN is injected together with ZIKV during a blood meal of the infected mosquito.  $\Delta$ LTRIN exists as a homodimer and its secondary structure remains unchanged regardless of the presence of Ca<sup>2+</sup>. The secondary structure exhibits resilience to varying temperatures, allowing  $\Delta$ LTRIN to maintain its full functionality from mosquito (22 °C) to human host (37 °C). The interacting sequence of  $\Delta$ LTRIN is identified by HDX-MS with sequence <sup>91</sup>QEKAHIAEHMDVPIDTSKMSEQELQFH<sup>118</sup> from the N-terminal. Illustration created with [BioRender.com](https://www.biorender.com).

**Supplementary Materials:** The following supporting information can be downloaded at: <https://www.mdpi.com/article/10.3390/biology13010042/s1>, Figure S1: (a) Sedimentation equilibrium analysis of  $\Delta$ LTRIN indicates that it exists in dimer formation. (b) Dynamic light scattering data (DLS) of  $\Delta$ LTRIN across different concentration. (c) Size exclusion chromatography elution profile and SDS-PAGE of  $\Delta$ LTRIN in the presence of  $\text{Ca}^{2+}$  or EGTA. (d) Comparing the DLS data of  $\Delta$ LTRIN in the presence of  $\text{Ca}^{2+}$  or EGTA. (e) Size exclusion chromatography elution profile and SDS-PAGE C133Q  $\Delta$ LTRIN. (f) DLS data of C133Q  $\Delta$ LTRIN showing that it is in dimer form. (g) The CD spectra of  $\Delta$ LTRIN in the presence of 10 mM EGTA continue to exhibit a predominant alpha helix secondary structure. (h) Secondary structure prediction of full length LTRIN by PSIPRED. The signal peptide is highlighted in red box. The  $\Delta$ LTRIN used is underlined with green; Figure S2: The EF-hand motif of  $\Delta$ LTRIN (a)  $\text{Ca}^{2+}$  binding ability of  $\Delta$ LTRIN is visualised using ruthenium red staining. (b) Gel mobility shift assay of  $\Delta$ LTRIN shows that limited structural changes are induced upon bind with  $\text{Ca}^{2+}$ . (c)  $\Delta$ LTRIN shows different binding affinity towards different divalent ions. (d) The presence of  $\text{Zn}^{2+}$  causes protein precipitation, resulting in a negative outcome; Table S1: The CD spectra of  $\Delta$ LTRIN in the presence of 2 mM  $\text{CaCl}_2$  is employed to assess its secondary structure content through three different methods (SELCON3, CONTINLL, and CDSSTR). The proportion of alpha-helix and loop structures in  $\Delta$ LTRIN as anticipated by AlphaFold was also quantified.

**Author Contributions:** Writing—original draft preparation, S.N.L. and J.S.; writing—review and editing, S.N.L., E.G., R.M.K., Y.K.M. and J.S.; data curation, S.N.L. and X.S.L.; methodology, S.N.L., E.G., I.R.A., X.S.L.; investigation, S.N.L.; conceptualization, S.N.L., Y.K.M. and J.S.; funding acquisition, R.M.K., Y.K.M. and J.S. All authors have read and agreed to the published version of the manuscript.

**Funding:** This work was supported by the Ministry of Education, Singapore (grant number WBS A-8000477-00-00).

**Institutional Review Board Statement:** Not applicable.

**Informed Consent Statement:** Not applicable.

**Data Availability Statement:** Data are contained within the article and Supplementary Materials.

**Acknowledgments:** S.N.L. is a graduate scholar in receipt of the National University research scholarship.

**Conflicts of Interest:** The authors declare that they have no conflict of interest.

## References

1. Caraballo, H.; King, K. Emergency department management of mosquito-borne illness: Malaria, dengue, and West Nile virus. *Emerg. Med. Pract.* **2014**, *16*, 1–23. [PubMed]
2. Franklino, L.H.V.; Jones, K.E.; Redding, D.W.; Abubakar, I. The effect of global change on mosquito-borne disease. *Lancet Infect. Dis.* **2019**, *19*, e302–e312. [CrossRef] [PubMed]
3. Mittal, S.; Federman, H.G.; Sievert, D.; Gleeson, J.G. The Neurobiology of Modern Viral Scourges: ZIKV and COVID-19. *Neuroscientist* **2021**, *28*, 438–452. [CrossRef]
4. Sun, P.; Nie, K.; Zhu, Y.; Liu, Y.; Wu, P.; Liu, Z.; Du, S.; Fan, H.; Chen, C.-H.; Zhang, R.; et al. A mosquito salivary protein promotes flavivirus transmission by activation of autophagy. *Nat. Commun.* **2020**, *11*, 260. [CrossRef] [PubMed]
5. Rocklöv, J.; Dubrow, R. Climate change: An enduring challenge for vector-borne disease prevention and control. *Nat. Immunol.* **2020**, *21*, 479–483. [CrossRef]
6. Guerrero, D.; Cantaert, T.; Missé, D. Aedes Mosquito Salivary Components and Their Effect on the Immune Response to Arboviruses. *Front. Cell. Infect. Microbiol.* **2020**, *10*, 407. [CrossRef]
7. Valenzuela-Leon, P.C.; Shrivastava, G.; Martin-Martin, I.; Cardenas, J.C.; Londono-Renteria, B.; Calvo, E. Multiple Salivary Proteins from Aedes aegypti Mosquito Bind to the Zika Virus Envelope Protein. *Viruses* **2022**, *14*, 221. [CrossRef]
8. Isawa, H.; Yuda, M.; Orito, Y.; Chinzei, Y. A mosquito salivary protein inhibits activation of the plasma contact system by binding to factor XII and high molecular weight kininogen. *J. Biol. Chem.* **2002**, *277*, 27651–27658. [CrossRef]
9. Hastings, A.K.; Uraki, R.; Gaitsch, H.; Dhaliwal, K.; Stanley, S.; Sproch, H.; Williamson, E.; MacNeil, T.; Marin-Lopez, A.; Hwang, J.; et al. Aedes aegypti NeSt1 Protein Enhances Zika Virus Pathogenesis by Activating Neutrophils. *J. Virol.* **2019**, *93*, e00395-19. [CrossRef]
10. Marin-Lopez, A.; Wang, Y.; Jiang, J.; Ledizet, M.; Fikrig, E. AgBR1 and NeSt1 antisera protect mice from Aedes aegypti-borne Zika infection. *Vaccine* **2021**, *39*, 1675–1679. [CrossRef]

11. Pielnaa, P.; Al-Saadawe, M.; Saro, A.; Dama, M.F.; Zhou, M.; Huang, Y.; Huang, J.; Xia, Z. Zika virus-spread, epidemiology, genome, transmission cycle, clinical manifestation, associated challenges, vaccine and antiviral drug development. *Virology* **2020**, *543*, 34–42. [[CrossRef](#)] [[PubMed](#)]
12. Huang, Y.J.; Higgs, S.; Horne, K.M.; Vanlandingham, D.L. Flavivirus-mosquito interactions. *Viruses* **2014**, *6*, 4703–4730. [[CrossRef](#)]
13. Rodríguez de la Rosa, R.P.; Cano-Torres, J.O.; Rosales, S.; Kleinert, A.P.; Gómez, A.; George, F.; George, J.; Piedad García, M.; Nájera-Cancino, G.; Guerra-de-Blas, P.D.C.; et al. Guillain-Barré syndrome outbreak in Tapachula temporally associated with the Zika virus introduction in Southern Mexico. *Epidemiol. Infect.* **2022**, *150*, e181. [[CrossRef](#)] [[PubMed](#)]
14. Song, B.H.; Yun, S.I.; Woolley, M.; Lee, Y.M. Zika virus: History, epidemiology, transmission, and clinical presentation. *J. Neuroimmunol.* **2017**, *308*, 50–64. [[CrossRef](#)] [[PubMed](#)]
15. Deng, S.-Q.; Yang, X.; Wei, Y.; Chen, J.-T.; Wang, X.-J.; Peng, H.-J. A Review on Dengue Vaccine Development. *Vaccines* **2020**, *8*, 63. [[CrossRef](#)]
16. Xu, L.; Ma, Z.; Li, Y.; Pang, Z.; Xiao, S. Antibody dependent enhancement: Unavoidable problems in vaccine development. *Adv. Immunol.* **2021**, *151*, 99–133. [[CrossRef](#)]
17. Manning, J.E.; Oliveira, F.; Coutinho-Abreu, I.V.; Herbert, S.; Meneses, C.; Kamhawi, S.; Baus, H.A.; Han, A.; Czajkowski, L.; Rosas, L.A.; et al. Safety and immunogenicity of a mosquito saliva peptide-based vaccine: A randomised, placebo-controlled, double-blind, phase 1 trial. *Lancet* **2020**, *395*, 1998–2007. [[CrossRef](#)]
18. Chuang, Y.M.; Tang, X.D.; Fikrig, E. A Mosquito AgTRIO Monoclonal Antibody Reduces Early Plasmodium Infection of Mice. *Infect. Immun.* **2022**, *90*, e0035921. [[CrossRef](#)]
19. Jin, L.; Guo, X.; Shen, C.; Hao, X.; Sun, P.; Li, P.; Xu, T.; Hu, C.; Rose, O.; Zhou, H.; et al. Salivary factor LTRIN from *Aedes aegypti* facilitates the transmission of Zika virus by interfering with the lymphotoxin- $\beta$  receptor. *Nat. Immunol.* **2018**, *19*, 342–353. [[CrossRef](#)]
20. Sudhamsu, J.; Yin, J.; Chiang, E.Y.; Starovasnik, M.A.; Grogan, J.L.; Hymowitz, S.G. Dimerization of LT $\beta$ R by LT $\alpha$ 1 $\beta$ 2 is necessary and sufficient for signal transduction. *Proc. Natl. Acad. Sci. USA* **2013**, *110*, 19896–19901. [[CrossRef](#)]
21. Altschul, S.F.; Madden, T.L.; Schäffer, A.A.; Zhang, J.; Zhang, Z.; Miller, W.; Lipman, D.J. Gapped BLAST and PSI-BLAST: A new generation of protein database search programs. *Nucleic Acids Res.* **1997**, *25*, 3389–3402. [[CrossRef](#)] [[PubMed](#)]
22. Tamura, K.; Stecher, G.; Kumar, S. MEGA11: Molecular Evolutionary Genetics Analysis Version 11. *Mol. Biol. Evol.* **2021**, *38*, 3022–3027. [[CrossRef](#)] [[PubMed](#)]
23. Yamaguchi, H.; Miyazaki, M. Refolding Techniques for Recovering Biologically Active Recombinant Proteins from Inclusion Bodies. *Biomolecules* **2014**, *4*, 235–251. [[CrossRef](#)]
24. Stetefeld, J.; McKenna, S.A.; Patel, T.R. Dynamic light scattering: A practical guide and applications in biomedical sciences. *Biophys. Rev.* **2016**, *8*, 409–427. [[CrossRef](#)]
25. Anisuzzaman, C.W. Methods in Molecular Biology Calcium-Binding Proteins and RAGE From Structural Basics to Clinical Applications Longistatin, an EF-Hand Ca<sup>2+</sup>-Binding Protein from Vector Tick: Identification, Purification, and Characterization. In *Calcium-Binding Proteins and RAGE: Methods in Molecular Biology*; Humana Press: Totowa, NJ, USA, 2013; pp. 127–146. [[CrossRef](#)]
26. Ozohanics, O.; Ambrus, A. Hydrogen-Deuterium Exchange Mass Spectrometry: A Novel Structural Biology Approach to Structure, Dynamics and Interactions of Proteins and Their Complexes. *Life* **2020**, *10*, 286. [[CrossRef](#)] [[PubMed](#)]
27. Zhang, Y.; Liu, Z.; Zhang, B. Separate roles of LMAN1 and MCFD2 in ER-to-Golgi trafficking of FV and FVIII. *Blood Adv.* **2023**, *7*, 1286–1296. [[CrossRef](#)] [[PubMed](#)]
28. Batoulis, H.; Schmidt, T.H.; Weber, P.; Schloetel, J.-G.; Kandt, C.; Lang, T. Concentration Dependent Ion-Protein Interaction Patterns Underlying Protein Oligomerization Behaviours. *Sci. Rep.* **2016**, *6*, 24131. [[CrossRef](#)] [[PubMed](#)]
29. Bhattacharya, A.; Prajapati, R.; Chatterjee, S.; Mukherjee, T.K. Concentration-Dependent Reversible Self-Oligomerization of Serum Albumins through Intermolecular  $\beta$ -Sheet Formation. *Langmuir* **2014**, *30*, 14894–14904. [[CrossRef](#)]
30. Merten, J.A.; Schultz, K.M.; Klug, C.S. Concentration-dependent oligomerization and oligomeric arrangement of LptA. *Protein Sci.* **2012**, *21*, 211–218. [[CrossRef](#)]
31. Rotoli, S.M.; Jones, J.L.; Caradonna, S.J. Cysteine residues contribute to the dimerization and enzymatic activity of human nuclear dUTP nucleotidohydrolase (nDut). *Protein Sci.* **2018**, *27*, 1797–1809. [[CrossRef](#)]
32. Wiedemann, C.; Kumar, A.; Lang, A.; Ohlenschläger, O. Cysteines and Disulfide Bonds as Structure-Forming Units: Insights From Different Domains of Life and the Potential for Characterization by NMR. *Front. Chem.* **2020**, *8*, 280. [[CrossRef](#)] [[PubMed](#)]
33. Anisuzzaman; Islam, M.K.; Miyoshi, T.; Alim, M.A.; Hatta, T.; Yamaji, K.; Matsumoto, Y.; Fujisaki, K.; Tsuji, N. Longistatin, a novel EF-hand protein from the ixodid tick *Haemaphysalis longicornis*, is required for acquisition of host blood-meals. *Int. J. Parasitol.* **2010**, *40*, 721–729. [[CrossRef](#)] [[PubMed](#)]
34. De Jesus, M.C.; Ingle, B.L.; Barakat, K.A.; Shrestha, B.; Slavens, K.D.; Cundari, T.R.; Anderson, M.E. The role of strong electrostatic interactions at the dimer interface of human glutathione synthetase. *Protein J.* **2014**, *33*, 403–409. [[CrossRef](#)] [[PubMed](#)]
35. Gifford, J.L.; Walsh, M.P.; Vogel, H.J. Structures and metal-ion-binding properties of the Ca<sup>2+</sup>-binding helix-loop-helix EF-hand motifs. *Biochem. J.* **2007**, *405*, 199–221. [[CrossRef](#)]
36. Lewit-Bentley, A.; Réty, S. EF-hand calcium-binding proteins. *Curr. Opin. Struct. Biol.* **2000**, *10*, 637–643. [[CrossRef](#)] [[PubMed](#)]
37. Zhou, Y.; Yang, W.; Kirberger, M.; Lee, H.-W.; Ayalasomayajula, G.; Yang, J.J. Prediction of EF-hand calcium-binding proteins and analysis of bacterial EF-hand proteins. *Proteins Struct. Funct. Bioinform.* **2006**, *65*, 643–655. [[CrossRef](#)] [[PubMed](#)]

38. Day, I.S.; Reddy, V.S.; Shad Ali, G.; Reddy, A.S. Analysis of EF-hand-containing proteins in Arabidopsis. *Genome Biol.* **2002**, *3*, research0056. [[CrossRef](#)]
39. Charuk, J.H.; Pirraglia, C.A.; Reithmeier, R.A. Interaction of ruthenium red with Ca<sup>2+</sup>-binding proteins. *Anal. Biochem.* **1990**, *188*, 123–131. [[CrossRef](#)]
40. Grabarek, Z. Insights into modulation of calcium signaling by magnesium in calmodulin, troponin C and related EF-hand proteins. *Biochim. Biophys. Acta* **2011**, *1813*, 913–921. [[CrossRef](#)]
41. Mun, S.A.; Park, J.; Kang, J.Y.; Park, T.; Jin, M.; Yang, J.; Eom, S.H. Structural and biochemical insights into Zn(2+)-bound EF-hand proteins, EFhd1 and EFhd2. *IUCrj* **2023**, *10*, 233–245. [[CrossRef](#)]
42. Andrews, S.S.; Tretton, J. Physical Principles of Circular Dichroism. *J. Chem. Educ.* **2020**, *97*, 4370–4376. [[CrossRef](#)]
43. Sreerama, N.; Woody, R.W. Estimation of protein secondary structure from circular dichroism spectra: Comparison of CONTIN, SELCON, and CDSSTR methods with an expanded reference set. *Anal. Biochem.* **2000**, *287*, 252–260. [[CrossRef](#)] [[PubMed](#)]
44. Ware, C.F. Targeting lymphocyte activation through the lymphotoxin and LIGHT pathways. *Immunol. Rev.* **2008**, *223*, 186–201. [[CrossRef](#)]
45. Dutra, G.; Komuczki, D.; Jungbauer, A.; Satzer, P. Continuous capture of recombinant antibodies by ZnCl<sub>2</sub> precipitation without polyethylene glycol. *Eng. Life Sci.* **2020**, *20*, 265–274. [[CrossRef](#)] [[PubMed](#)]
46. Abou-Abbass, H.; Abou-El-Hassan, H.; Bahmad, H.; Zibara, K.; Zebian, A.; Youssef, R.; Ismail, J.; Zhu, R.; Zhou, S.; Dong, X.; et al. Glycosylation and other PTMs alterations in neurodegenerative diseases: Current status and future role in neurotrauma. *Electrophoresis* **2016**, *37*, 1549–1561. [[CrossRef](#)]
47. Gong, Y.; Qin, S.; Dai, L.; Tian, Z. The glycosylation in SARS-CoV-2 and its receptor ACE2. *Signal Transduct. Target. Ther.* **2021**, *6*, 396. [[CrossRef](#)]
48. Krautter, F.; Iqbal, A.J. Glycans and Glycan-Binding Proteins as Regulators and Potential Targets in Leukocyte Recruitment. *Front. Cell. Dev. Biol.* **2021**, *9*, 624082. [[CrossRef](#)]
49. Villalobo, A.; Ishida, H.; Vogel, H.J.; Berchtold, M.W. Calmodulin as a protein linker and a regulator of adaptor/scaffold proteins. *Biochim. Biophys. Acta* **2018**, *1865*, 507–521. [[CrossRef](#)]
50. Zhang, M.; Abrams, C.; Wang, L.; Gizzi, A.; He, L.; Lin, R.; Chen, Y.; Loll, P.J.; Pascal, J.M.; Zhang, J.F. Structural basis for calmodulin as a dynamic calcium sensor. *Structure* **2012**, *20*, 911–923. [[CrossRef](#)]
51. Halling, D.B.; Aracena-Parks, P.; Hamilton, S.L. Regulation of voltage-gated Ca<sup>2+</sup> channels by calmodulin. *Sci. STKE* **2005**, *2005*, re15. [[CrossRef](#)]
52. Zheng, C.; Liu, H.H.; Zhou, J.; Zhang, B. EF-hand domains of MCFD2 mediate interactions with both LMAN1 and coagulation factor V or VIII. *Blood* **2010**, *115*, 1081–1087. [[CrossRef](#)]
53. Guy, J.E.; Wigren, E.; Svärd, M.; Härd, T.; Lindqvist, Y. New Insights into Multiple Coagulation Factor Deficiency from the Solution Structure of Human MCFD2. *J. Mol. Biol.* **2008**, *381*, 941–955. [[CrossRef](#)] [[PubMed](#)]
54. Berggård, T.; Miron, S.; Önnarfjord, P.; Thulin, E.; Åkerfeldt, K.S.; Enghild, J.J.; Akke, M.; Linse, S. Calbindin D28k Exhibits Properties Characteristic of a Ca<sup>2+</sup> Sensor. *J. Biol. Chem.* **2002**, *277*, 16662–16672. [[CrossRef](#)] [[PubMed](#)]
55. Noble, J.W.; Almalki, R.; Roe, S.M.; Wagner, A.; Duman, R.; Atack, J.R. The X-ray structure of human calbindin-D28K: An improved model. *Acta Crystallogr. Sect. D Struct. Biol.* **2018**, *74*, 1008–1014. [[CrossRef](#)] [[PubMed](#)]
56. Lakowski, T.M.; Lee, G.M.; Okon, M.; Reid, R.E.; McIntosh, L.P. Calcium-induced folding of a fragment of calmodulin composed of EF-hands 2 and 3. *Protein Sci.* **2007**, *16*, 1119–1132. [[CrossRef](#)] [[PubMed](#)]
57. Huang, Y.; Zhou, Y.; Wong, H.C.; Chen, Y.; Chen, Y.; Wang, S.; Castiblanco, A.; Liu, A.; Yang, J.J. A single EF-hand isolated from STIM1 forms dimer in the absence and presence of Ca<sup>2+</sup>. *FEBS J.* **2009**, *276*, 5589–5597. [[CrossRef](#)] [[PubMed](#)]
58. Benoit, J.B.; Lopez-Martinez, G.; Patrick, K.R.; Phillips, Z.P.; Krause, T.B.; Denlinger, D.L. Drinking a hot blood meal elicits a protective heat shock response in mosquitoes. *Proc. Natl. Acad. Sci. USA* **2011**, *108*, 8026–8029. [[CrossRef](#)]
59. Ma, J.; Martin, J.D.; Zhang, H.; Auger, K.R.; Ho, T.F.; Kirkpatrick, R.B.; Grooms, M.H.; Johanson, K.O.; Tummino, P.J.; Copeland, R.A.; et al. A second p53 binding site in the central domain of Mdm2 is essential for p53 ubiquitination. *Biochemistry* **2006**, *45*, 9238–9245. [[CrossRef](#)]
60. Garg, R.; Juncadella, I.J.; Ramamoorthi, N.; Ashish; Ananthanarayanan, S.K.; Thomas, V.; Rincón, M.; Krueger, J.K.; Fikrig, E.; Yengo, C.M.; et al. Cutting edge: CD4 is the receptor for the tick saliva immunosuppressor, Salp15. *J. Immunol.* **2006**, *177*, 6579–6583. [[CrossRef](#)]

**Disclaimer/Publisher’s Note:** The statements, opinions and data contained in all publications are solely those of the individual author(s) and contributor(s) and not of MDPI and/or the editor(s). MDPI and/or the editor(s) disclaim responsibility for any injury to people or property resulting from any ideas, methods, instructions or products referred to in the content.